NASA Technical Memorandum 103104

Computational Experience With a Three-Dimensional Rotary Engine Combustion Model

M.S. Raju
Sverdrup Technology, Inc.
Lewis Research Center Group
Brook Park, Ohio

and

E.A. Willis
National Aeronautics and Space Administration
Lewis Research Center
Cleveland, Ohio

Prepared for the
Joint Symposium on General Aviation Systems
cosponsored by the AIAA and FAA
Ocean City, New Jersey, April 11-12, 1990

COMPUTATIONAL EXPERIENCE WITH A THREE-DIMENSIONAL ROTARY ENGINE COMBUSTION MODEL

M.S. Raju*
Sverdrup Technology, Inc.
Lewis Research Center Group
Brook Park, Ohio 44142

and

E.A. Willis†
National Aeronautics and Space Administration
Lewis Research Center
Cleveland, Ohio 44135

SUMMARY

A new computer code has been developed to analyze the chemically reactive flow and spray combustion processes occurring inside a stratified-charge rotary engine. Mathematical and numerical details of the new code were recently described by the present authors. This paper presents the results of limited, initial computational trials as a first step in a long-term assessment/validation process. The engine configuration studied was chosen to approximate existing rotary engine flow-visualization and hot-firing test rigs. Typical results include (1) pressure and temperature histories, (2) torque generated by the nonuniform pressure distribution within the chamber, (3) energy release rates, and (4) various flow-related phenomena. These are discussed and compared with other predictions reported in the literature. The adequacy or need for improvement in the spray/combustion models and the need for incorporating an appropriate turbulence model are also discussed.

INTRODUCTION

The rotary combustion engine (RCE) would be a desirable powerplant for light aircraft, drones, auxiliary and ground power units, and marine and industrial applications if its efficiency could be made closer to that of diesel engines. It has inherent advantages over reciprocating engines such as higher airflow capacity, higher power-to-weight ratio, low frontal area, and less vibration. An initial attempt to introduce a gasoline-fueled rotary engine into the general aviation market in the mid 1970's was unsuccessful, however, because of poor fuel economy, uncertain availability of avgas, and marginal weight advantage over contemporary reciprocating engines. Subsequent research sponsored by industry, NASA, and the Navy has led to the development of the stratified-charge rotary engine (SCRE) concept. This work has already demonstrated a substantial improvement in specific power, multifuel capability, and a reduction of cruise brake specific fuel consumption (BSFC) from over 0.5 lb/bhp-hr to a value approaching 0.41 lb/bhp-hr. A major factor in this improvement was the use of Computational Fluid Dynamics (CFD) methods to

---

*Senior Research Engineer, Member AIAA.
†Chief Engineer, Propulsion Systems Division, Member AIAA.

analyze the airflow, spray, and combustion events of the RCE. Continuing research and development sponsored by NASA is aimed at further reducing the cruise BSFC, from the current value to 0.35 or less, by the end of 1992. Much of the expected improvement will be enabled by further CFD-driven fuel injection, spray and nozzle optimization, rotor pocket reshaping and relocation, and related changes. Thus, the availability of accurate, reliable, and fast operating CFD simulations of the RCE internal processes is clearly a key element in the future development of this promising engine concept.

Early modeling efforts on the Wankel engine were based on thermodynamic models (refs. 1 and 2) and also on one-dimensional modeling of premixed-charge combustion (ref. 3). Multidimensional models of the Wankel engine are of more recent origin. Grasso et al. (ref. 4) presented the first three-dimensional computations of an SCRE during the early stages of flame propagation. Subsequent computations performed by Abraham and Bracco (refs. 5 and 6) led to some important design changes in the rotary engine development at Deere and Co., especially in the fuel injector configuration. Their code, REC-3D-FSC-86, is a modified version of the KIVA code developed at Los Alamos National Laboratory (ref. 7) for the modeling of reciprocating engines. KIVA makes use of a conditionally stable algorithm, and the stability of the KIVA scheme is improved by making use of an acoustic subcycling step in order to alleviate the stiffness problems arising from compressibility effects. There appears to be considerable room for improvement in the code, since it neglects the spatial gradients whenever the grid spacing becomes smaller than some predefined value and also requires excessive CPU time when the engine speed becomes small. Shih et al. (ref. 8) presented the first two-dimensional computations of a motored Wankel engine in the absence of combustion. Their code, LEWIS-2D, is based on the Beam-Warming type of alternating-direction implicit (ADI) method. Their computations were subsequently extended to three dimensions in Steinthorsson et al. (ref. 9). Linear stability analysis has shown that the ADI method is unconditionally stable in two dimensions but is unconditionally unstable in three dimensions. Although artificial dissipation has some stabilizing effect, an excessive amount can impair stability and reduce accuracy and convergence. Recently, Li et al. (ref. 10) modified their LEWIS-3D code based on upwind schemes together with the incorporation of a k-ϵ turbulence model.

The present solution procedure differs from the above in terms of the numerics and the submodels used for turbulence, combustion, and sprays. Mathematical and numerical details of the new code were recently described by the present authors (ref. 11). This paper presents the results of limited, initial computational trials as a first step in a long-term assessment/validation process. The engine configuration studied was chosen to approximate existing rotary engine test rigs. Representative results - in terms of pressure and temperature histories, torque generated due to the nonuniform pressure distribution within the chamber, energy release rates, and various flow-related phenomena - are discussed in comparison with other predictions reported to date in the literature. The objective is to evaluate the adequacy or need for improvement in the spray/combustion models and to assess the need for incorporating an appropriate turbulence model.

PHYSICAL DESCRIPTION

A schematic of the Wankel engine is shown in figure 1. The Wankel engine is composed of a trochoid housing (ref. 1) with peripheral intake and exhaust ports, fuel injector and spark igniter, a three-flank rotor, and a crankshaft. The contour of the inner surface of the outer casing of the Wankel engine is a two-lobe peritrochoid. The contour of a rotor revolving along an outer housing is a peritrochoid inner envelope. The rotor surface is modified to include rotor pockets (refs. 2 to 4). The presence of the rotor pockets not only alters the expansion and compression ratio of the engine, but also plays an important role in modifying its internal flowfield, mixing, and combustion characteristics.

The present rotor configuration is adopted from Steinthorsson et al. (ref. 9). In its other dimensions, the engine has a generating radius, R, of 0.1064 m; eccentricity, E, of 0.01542 m; clearance, C, of 0.004 m; chamber width, W, of 0.07 m; and port width, W_p, of 0.05 m. These dimensions give rise to maximum and minimum volumes of 750 and 115 cm^3, respectively, thereby yielding a compression ratio of about 6.5.

The rotor turns eccentrically at one third of the crankshaft speed. The three combustion chambers of the Wankel engine are the three regions enclosed between the three rotor faces and the peritrochoid housing, two side housings, two side seals, and lead and lag apex seals. In the present calculations, only one of the three combustion chambers is considered, since leakage through the seals is assumed to be negligible. As the rotor revolves around the crankshaft, each of the combustion chambers is continually deformed. This produces the necessary compression and expansion of the fluid for the required engine performance during each cyclic operation.

It should be noted that each combustion chamber has two minimum and maximum volume positions. Hence, the top-dead-center (TDC) and bottom-dead-center (BDC) positions are defined differently than would be the case in a reciprocating engine, and it will be important to keep the following conventions in mind. In this study, a crank angle of zero radians corresponds with the minimum volume that occurs near the ports. This position is referred to as the BDC. The other position, corresponding with the minimum volume near the fuel injector location, is referred to as the TDC. Thus, combustion occurs near TDC as in a reciprocating engine, but the BDC position has a different meaning.

The exhaust port opens at a crank angle of 5.96 rad before BDC and closes at 1.07 rad after BDC, and the exhaust back-pressure is maintained at 0.85 atm. The intake port opens at 1.26 rad before BDC and closes at 5.96 rad after BDC. Fresh air enters through the intake while the intake stagnation temperature $T_{s,int}$ and static pressure P_{int} are maintained at 400 K and 1.25 atm, respectively. The fuel injector has eight holes and is located near the middle of the trochoid housing as shown in figure 1. The fuel emerges in a fan-shaped pattern consisting of eight sprays. The initial spray distribution is given by a Rosen-Ramler distribution with the initial droplet sizes ranging from $10\ \mu m \leq r_{k,i} \leq 30\ \mu m$. The initial droplet velocity and temperature are taken to be 100 m/s and 300 K, respectively. The fuel injection begins at 8.6 rad after BDC and ends at 9.25 rad after BDC. The liquid fuel injection is simulated by injecting a specified number of discretized parcels of fixed mass associated with a given droplet-size group at uniform intervals corresponding with the fuel-injection time step. The ignition process begins at 8.65 rad after BDC and ends at 8.75 rad after BDC. The ignition spark is simulated by raising the temperature of a few nodes of the computational domain on the wall at the spark ignitor location from 400 to 1500 K. A complete physical description of the engine is provided in our earlier paper (ref. 11).

RESULTS AND DISCUSSION

Numerical solutions were obtained for the engine flowfield under motoring conditions for a single case with all of the ports closed; they were also obtained under firing conditions for two cases, with equivalence ratios of 0.45 and 0.75. For all cases, the computations were initiated before the opening of the exhaust port for only one of the three chambers (formed with the second rotor flank as shown in fig. 1). Here we present the results obtained for the three different cases for an engine speed of 4000 rpm. The temperatures of the rotor and housing surfaces were maintained at 300 K for the case considered under motoring conditions and at 400 K for the firing conditions. The initial conditions correspond to the conditions of quiescent air at a pressure, P_{in}, of 1 atm and a temperature, T_{in}, of 300 K for the motoring engine and at 1 atm and 400 K for the firing engine.

All of the computations were performed with a uniform time-step size such that 15 000 time-steps span the 6π radians of one entire rotor cyclic-rotation. The calculations were performed on a grid with a mesh size of $i = 31$, $j = 16$, and $k = 20$, where i, j, and k represent the coordinate surfaces in the direction extending from the trailing-edge surface to the leading-edge surface of the combustor, from the rotor to the housing surface, and from the side wall to the symmetry plane of the domain between the end-to-end side walls, respectively.

Motoring Results

The usefulness of any numerical scheme lies in its ability to generate meaningful predictions for a wide variety of engine operating conditions. Both the numerics and the models used for turbulence, combustion, and sprays determine the accuracy of the predictions. The selection of a finite-difference formulation is mainly dictated by a careful balance between the numerical stability, efficiency, and accuracy considerations for the problem under consideration. Stability is often achieved at the expense of accuracy and efficiency. It is also instructive to note that a numerical scheme is often made stable either by explicitly adding some amount of artificial dissipation, or by the numerical dissipation that inherently arises from a given finite difference formulation. For the predictions to be meaningful, the numerical dissipation required for stability considerations should be small compared with the dissipation arising from the actual physical processes governing the flowfield.

The best way to assess the accuracy of a numerical scheme is to compare the predictions with experimental data. In our previous paper (ref. 11) a good measure of qualitative agreement was noted between the predictions and an experimental flow-visualization pattern during the intake process. In the absence of applicable experimental data on the average pressure and temperature variation versus crank angle, a numerical experiment was performed for a motoring engine with all of the ports closed. This allowed comparisons between the predictions and the corresponding isentropic results to be made.

Figure 2 shows the computed mass-averaged temperature and volume-averaged pressure versus crank angle. Also shown in the figure are the corresponding results obtained from isentropic conditions, with an exponent of 1.4. The computations predicted a temperature of 490 K and a pressure of 8.4 atm at TDC. The corresponding differences from the isentropic conditions are 15.8 and 23 percent, respectively. Although it is hard to ascertain the validity of the predictions in the absence of any experimental data, the observed differences between the isentropic conditions and the predictions can be explained by the following reasons:

(1) Both the stagnation pressure and temperature would be slightly higher than the corresponding static conditions near TDC, since the flow velocities at this position approach 50 m/sec.

(2) Viscous effects become increasingly significant near TDC since the surface area to volume ratio becomes very large near the clearance regions of the apex seals and also because of a strong squish flow resulting from the nonuniform pressure distribution. The squish flow is a unique feature of the rotary engines that has no counterpart in reciprocating engines.

(3) The heat losses to the walls also contribute to the observed differences since the temperature of the walls is maintained at 300 K.

(4) Because of the shape of the combustion chamber, all the gas within it may not undergo the same degree of expansion or compression simultaneously. In fact, while some gas undergoes compression other gas is likely to undergo expansion as the rotor moves around TDC. This process enhances the convective heat transfer to the walls.

(5) Numerical dissipation is also likely to contribute to the observed differences. Li et al. (ref. 10) made similar comparisons between the various numerical schemes studied for a two-dimensional motoring engine. We have not attempted to make any direct comparisons with their predictions because of the different engine configurations used in the respective studies. At the end of the computations the predictions indicate there is an accumulation of mass by about 3 percent. Even though our governing equations are formulated in a strong-conservation law form (ref. 11), the way in which the boundary conditions are implemented makes the finite-difference formulation weakly conservative. However, the observed discrepancy in mass could be reduced further by increasing the number of grid points in the computational domain.

Figure 3 shows the computed torque about the center of the rotor (as opposed to output torque about the center of the crankshaft). This is generated in part by the nonuniform pressure distribution on the rotor surface and in part by a difference of the pressure forces acting on the trailing and leading apex seals. If a uniform pressure prevailed throughout the combustion chamber, the resulting torque would be zero. However, the effect of pressure nonuniformity clearly results in a negative torque contribution opposing the rotor motion. Hence, work needs to be performed to overcome this torque induced by the nonuniform pressure distribution. From the predictions, it is evident that the pressure becomes more nonuniform near TDC and, in fact, the torque has a maximum negative value at this location. The corresponding values of the torque averaged over one cyclic period is found to be -0.9357 Nm (rotor) and -0.1259 Nm (seals).

To provide a better understanding of the observed nonuniformities in the flowfield, the pressure and temperature contours together with the flow velocity at the symmetric plane k = 19 and crank angle of 19.3 rad are shown in figure 4. In the isocontour plots, the isocontour lines near the maximum are shown as dotted lines and near the minimum are shown as solid lines. In the velocity vector plot, only three different sizes of arrow symbols are used to distinguish the variation between the maximum and minimum values. Both the pressure and temperature have a maximum value in the region near the trailing apex seal, and the flow velocity is essentially determined by the rotor movement.

Firing Results

In this section we present the results for two other cases that were conducted under firing conditions, for which the operating parameters were described earlier in the paper. The fuel/air equivalence ratio, Φ, is taken to be 0.45 for one case and 0.75 for the other.

Here we first present the results of the three-dimensional computations describing the overall behavior of the combustor in terms of the volume-averaged pressure versus combustor volume (p-v diagrams). This includes the variation of mass-averaged temperature, the torque due to pressure nonuniformity, and vaporization and combustion rates versus crank angle. Then we proceed to examine the flowfield in detail during the fuel vaporization and combustion processes. The details of the flowfield during the opening of the exhaust and/or intake are presented in detail in our earlier paper (ref. 11).

The computations are initiated just before the exhaust port opens. The initial pressure and temperature of the gas are taken to be 1 atm and 400 K, respectively. After the exhaust port opens the residual gas moves out of the combustion chamber, since the imposed pressure of 0.85 atm in the exhaust remains lower than the interior engine pressure during most of the compression cycle. Both the engine pressure and temperature remain fairly uniform during the exhaust process, as shown in figure 5. As the rotor moves farther, the intake port opens and fresh air moves into the combustion chamber. Most of the intake process occurs during the expansion stroke of the engine. The slight rise in the pressure during the intake process merely reflects the intake pressure, which is maintained at 1.25 atm.

After the intake port closes, the gas undergoes nearly isentropic compression until combustion begins. During the combustion process, both the pressure and temperature rise sharply to about 33 atm and 1450 K, reaching their maximum values near TDC. During the expansion stroke, the gas undergoes nearly isentropic expansion until the exhaust port opens again. Both the pressure and temperature fall off sharply until the interior pressure near the exhaust port reduces to a value below the imposed exhaust back-pressure of 0.85 atm. When this condition is reached near a crank angle of 16 rad, the temperature remains fairly uniform at 650 K for a brief period before the intake charge at 400 K enters the chamber. The temperature falls to 400 K during the remainder of the opening of the intake port.

The torque variation versus crank angle in figure 6(a) shows that the pressure distribution on the rotor surface undergoes a kind of beating phenomenon associated with acoustic resonance during the intake and/or exhaust port opening period. It is also noteworthy that positive torque is generated during the overlapping period in which both the exhaust and intake ports are open simultaneously. Once again, the maximum negative torque is generated near the minimum volume as in the motoring case. The corresponding values of the torque, averaged over one cycle, are found to be -0.817 Nm (rotor) and 0.508 Nm (seals). Comparison with the previous case shows that the average rotor torque due to the pressure nonuniformity under both motoring and firing cases has a similar value. This indicates that the resulting pressure gradient on the rotor surface is a result of the fluid motion associated with the rotor movement. However, the average torque due to pressure acting on the seals for a firing engine is found to be positive whereas it had a negative value for the motoring case.

Figure 6(b) shows the crank angle variation of the evaporated fuel and also the amount of reacted fuel. The total amount of liquid fuel injected is equal to 0.23 g, which corresponds to an equivalence ratio of about 0.45. The slope of these curves indicates that most of the fuel, after it evaporates, reacts quickly with oxidizer to form products. This in turn implies that most of the fuel burns as if in a premixed-flame environment. Although the validity of the results can be verified only after proper experimental data is made available, the extremely fast combustion rates observed in the present study are in contradiction to the numerical predictions presented by Abraham et al. (ref. 5), in which they reported lower rates for both fuel vaporization and combustion. Our present computations are based on the assumption of laminar fluid motion and chemical kinetics. In a turbulent reacting flow, the combustion rates are normally rate-controlled by the mixing rate rather than the Arrhenius reaction rate (ref. 12). Also one expects to predict lower temperatures for the gas near the walls, when the effect of turbulence is properly accounted for in the heat transfer calculations. This, in turn, might reduce both the vaporization and combustion rates.

The effect of increasing the equivalence ratio from 0.45 to 0.75 is shown in figures 7 and 8. Although the qualitative behavior for both cases remains the same, the increase in heat input, as a result of increasing the fuel content, is shown to result in an increase in the maximum temperature and pressure observed from 1450 to 1750 K and 33 to 44 atm, respectively.

Flowfield Phenomena

We now turn our attention to the details of the flowfield at the beginning of, during, and after the combustion and vaporization for the case with an equivalence ratio of 0.75. Figure 9 shows the isocontours of pressure and temperature, and the velocity vector plot at a crank angle of 8.6 rad. This is before the fuel injection begins. Both the pressure and temperature distributions remain fairly uniform in the region extending all the way from the trailing apex seal to the end of the rotor pocket near the leading apex seal. The maximum values for the pressure and temperature are observed to occur within this region. Fairly large gradients in the distribution of both temperature and pressure are also observed in the clearance region near the leading apex seal. The fluid motion is shown to be strongly influenced by the rotor movement.

Figures 10 to 12 show the droplet trajectories; the isocontour lines of fuel, oxidizer, carbon dioxide, and temperature; and the velocity vector plot at a crank angle of 9.3. The figures showing the rotor pocket cross section are drawn in an elongated scale compared with the others in order to provide a better graphic illustration of the results. The polydisperse character of the spray is represented by different sized circles which are indicative of the size of the initial droplets. Although the particles retain the fan-shape configuration during this later part of the fuel vaporization process, the deflection of the particles in the direction of the gaseous flow is evident from the path originally dictated by the particle initial conditions.

A very small region near the fuel injector location is found to be fuel rich. Whereas stratified charge gives rise to a gaseous diffusion flame, a careful examination of figure 10 also reveals an absence of fuel concentration in the region near the rotor pocket surface where fuel concentration is expected otherwise from the presence of liquid fuel in that region. It is more likely that the combustion characteristics in that region are influenced by an isolated combusting droplet behavior. The oxygen concentration is found to be lower near the high temperature region than in the regions near the seals. An opposite trend is observed for the carbon dioxide distribution. The temperature in the flame region is around 3106 K and on the walls is 400 K. Again the fluid motion is found to be essentially dictated by the rotor motion.

During the expansion stroke, after the combustion is completed, the distributions of temperature and of oxidizer and carbon dioxide concentrations are found to become fairly uniform throughout the chamber as shown in figure 13.

CONCLUDING REMARKS

We have presented preliminary results for a Wankel engine under both motoring and firing conditions, obtained from the solution of unsteady, three-dimensional Navier-Stokes equations. These results are based on the assumption of laminar fluid motion and chemical kinetics, with the use of appropriate submodels for combustion and sprays.

The results show the average rotor torque generated by the nonuniform pressure distribution is nearly the same for the different cases considered under both motoring and firing conditions. This indicates that the pressure nonuniformity is determined mostly by the rotor-induced fluid motion. The pressure is higher near the trailing apex region than near the leading apex region.

One indication of our study is that, under the present assumptions, vaporization appears to be more rate-controlling than mixing during the combustion process. This finding is contrary to the numerical predictions reported by Abraham et al. (ref. 5). While considering the fact that the present engine configuration is somewhat different from the one used in their studies, it should be noted again that the present computations are performed without attempting to describe the turbulent aspect of the fluid motion. Both the heat transfer, fluid mechanics, and combustion characteristics in a engine flowfield will be influenced strongly by the turbulent fluid motion. Our solution procedure is currently being modified to include an appropriate turbulence model.

The code takes about 10 CPU hours on a CRAY Y-MP, when the calculations are performed on a 31 by 16 by 20 grid. This covers one entire cyclic period of 6π rads for a firing case. It appears that we are the first to have reported numerical predictions obtained from three-dimensional computations in terms of pressure, temperature, and torque histories for an entire cyclic period. The code appears to be potentially very efficient compared with the other schemes used in modeling Wankel engines.

REFERENCES

1. Danieli, G.A.; Keck, J.C.; and Heywood, J.B.: Experimental and Theoretical Analysis of Wankel Engine Performance. SAE Paper 780416, 1978.
2. Roberts, J.A.; Norman, T.J.; Ekchian, J.A.; and Heywood, J.B.: Computer Models for Evaluating Premixed and DISC Wankel Engine Performance. SAE Paper 860613, 1986.
3. Bracco, F.V.; and Sirignano, W.A.: Theoretical Analysis of Wankel Engine Combustion. Combustion Science and Technology, vol. 7, no. 3, 1973, pp. 109-123.
4. Grasso, F.; Wey, M-J.; Bracco, F.V.; and Abraham, J.: Three-Dimensional Computations of Flows in a Stratified-Charge Rotary Engine. SAE Paper 870409, 1987.
5. Abraham, J.; Wey, M-J.; and Bracco, F.V.: Pressure Non-Uniformity and Mixing Characteristics in a Stratified Charge Rotary Engine Combustion. SAE Paper 880624, 1988.
6. Abraham, J.; and Bracco, F.V.: Comparison of Computed and Measured Pressure in a Premixed-Charge Natural-Gas-Fueled Rotary Engine. Rotary Engine Design: Analysis and Developments, SAE SP-768, SAE, Warrendale, PA, 1989, pp. 117-131.
7. Amsden, A.A.; Ramshaw, J.D.; O'Rourke, P.J.; and Dukowicz, J.K.: KIVA: A Computer Program for Two- and Three-Dimensional Fluid Flows With Chemical Reactions and Fuel Sprays. LA-10245-MS, Los Alamos National Laboratory, Feb. 1985.
8. Shih, T.I.-P; Yang, S.-L; and Schock, H.J.: A Two-Dimensional Numerical Study of the Flow Inside the Combustion Chamber of a Motored Rotary Engine. SAE Paper 860615, 1986.
9. Steinthorsson, E.; Shih, T.I-P.; Schock, H.J.; and Stegeman, J.: Calculations of the Unsteady, Three-Dimensional Flow Field Inside a Motored Wankel Engine. SAE Paper 880625, 1988.
10. Li, Z.; Steinthorsson, E.; Shih, T.I.-P.; and Nguyen, H.L.: Modelling and Simulation of Wankel Engine Flow Fields. SAE Paper 900029, 1990.
11. Raju, M.S.; and Willis, E.A.: Analysis of Rotary Engine Combustion Processes Based on Unsteady, Three-Dimensional Computations. AIAA Paper 90-0643, 1990.
12. Raju, M.S.; and Sirignano, W.A.: Multicomponent Spray Computations in a Modified Centerbody Combustor. AIAA Paper 88-0638, 1988.

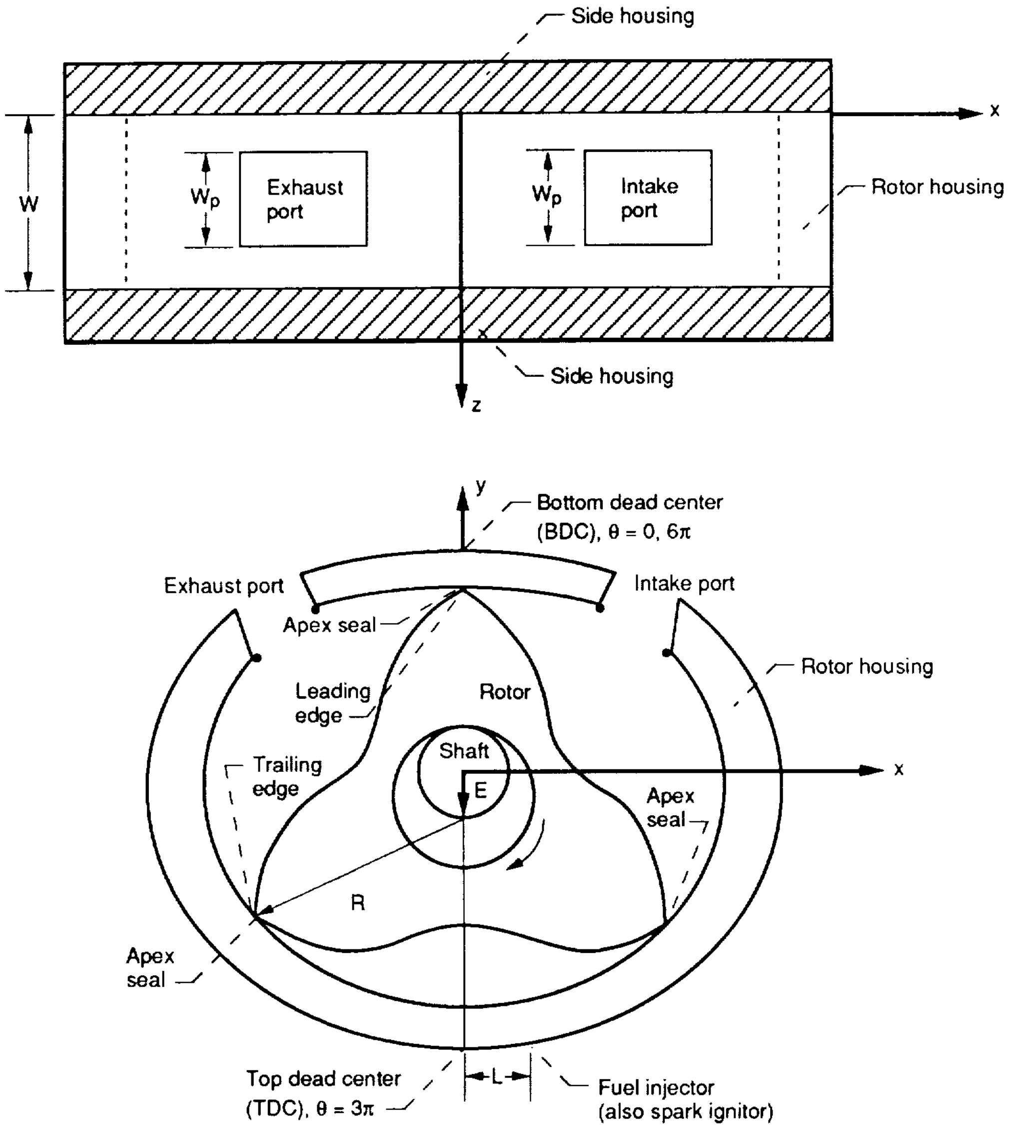

Figure 1.—Schematic of the Wankel engine that was studied.

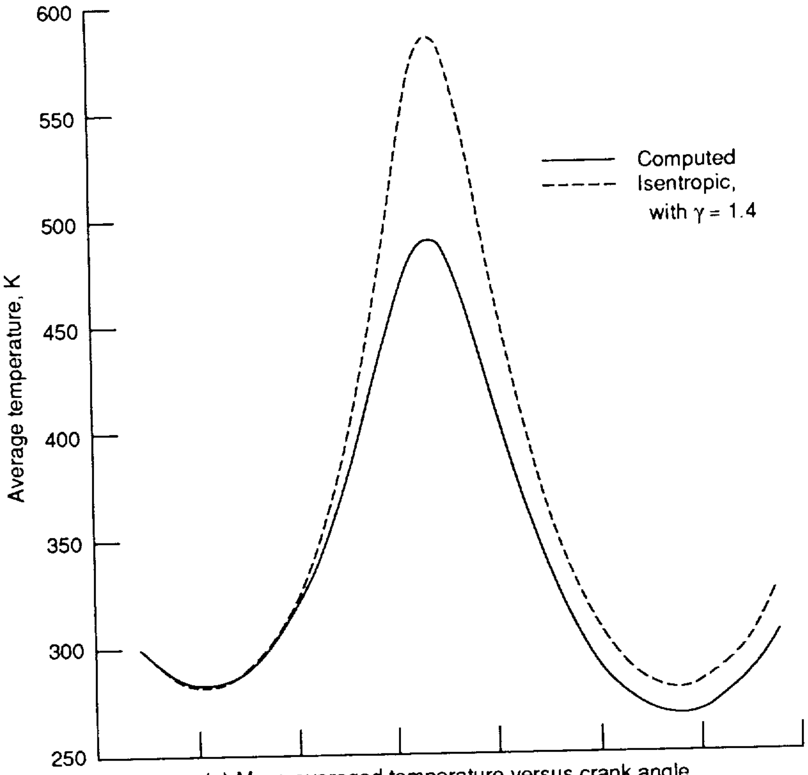

(a) Mass-averaged temperature versus crank angle.

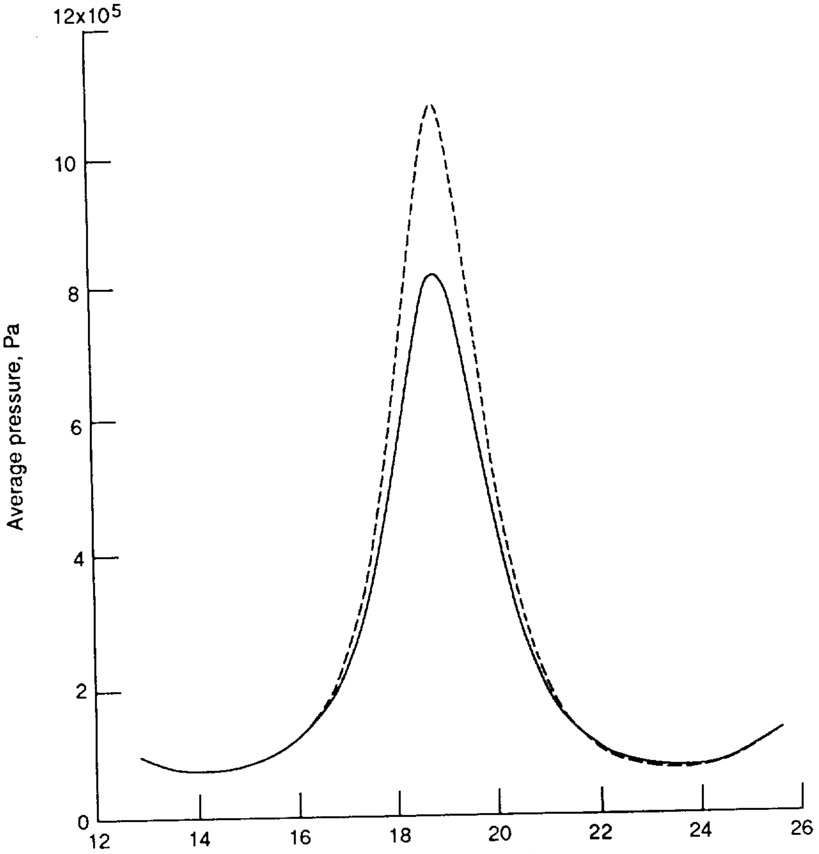

(b) Volume-averaged pressure versus crank angle.

Figure 2.—Motoring results with all ports closed.

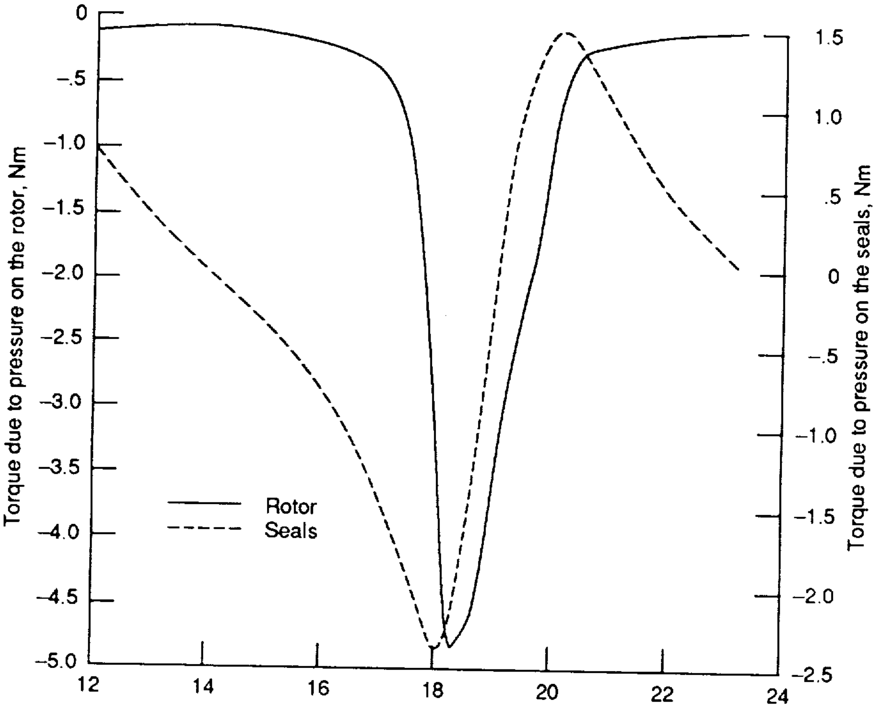

Figure 3.—Torque versus crank angle with all ports closed.

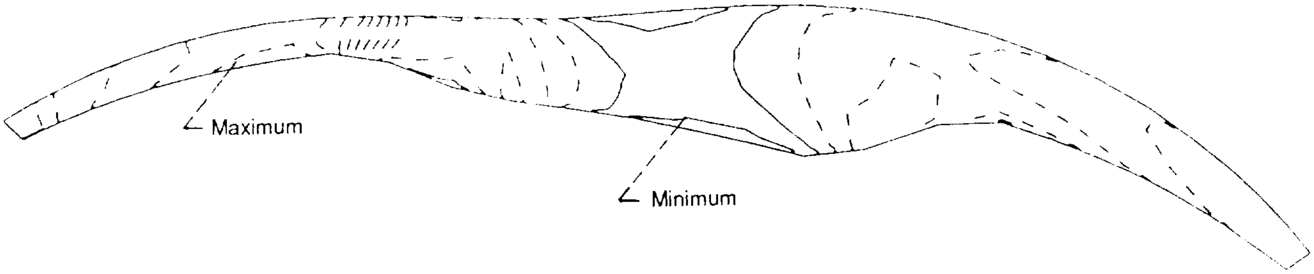

(a) Pressure contours ($P_{max} = 0.77x10^6$, $P_{min} = 0.74x10^6$, and $\Delta P = 0.21x10^4$).

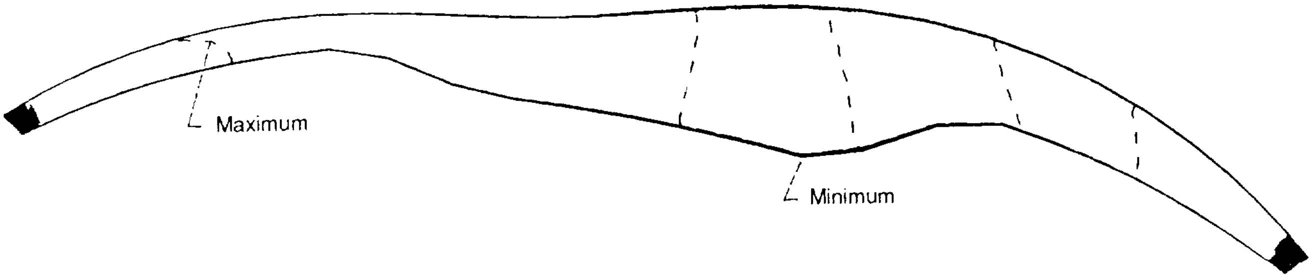

(b) Temperature contours ($T_{max} = 479.4$, $T_{min} = 300$, and $\Delta T = 5$).

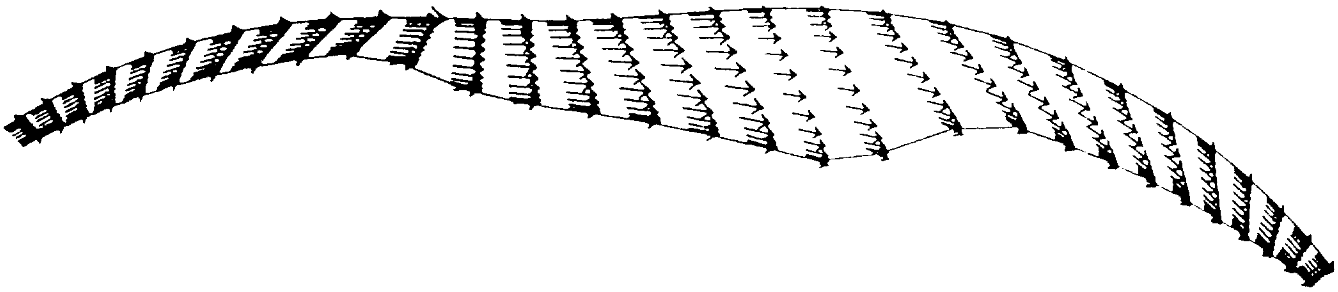

(c) Velocity vector plot ($V_{max} = 43.8$ m/s).

Figure 4.—Gas pressure, temperature, and velocity at $\theta = 19.3$ rad and $K = 19$ with all ports closed.

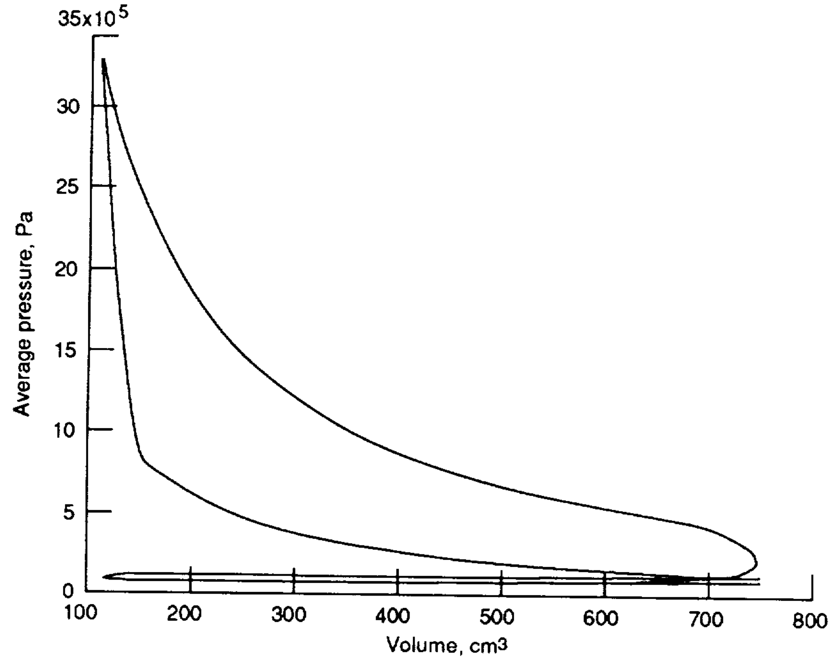

(a) Pressure versus volume.

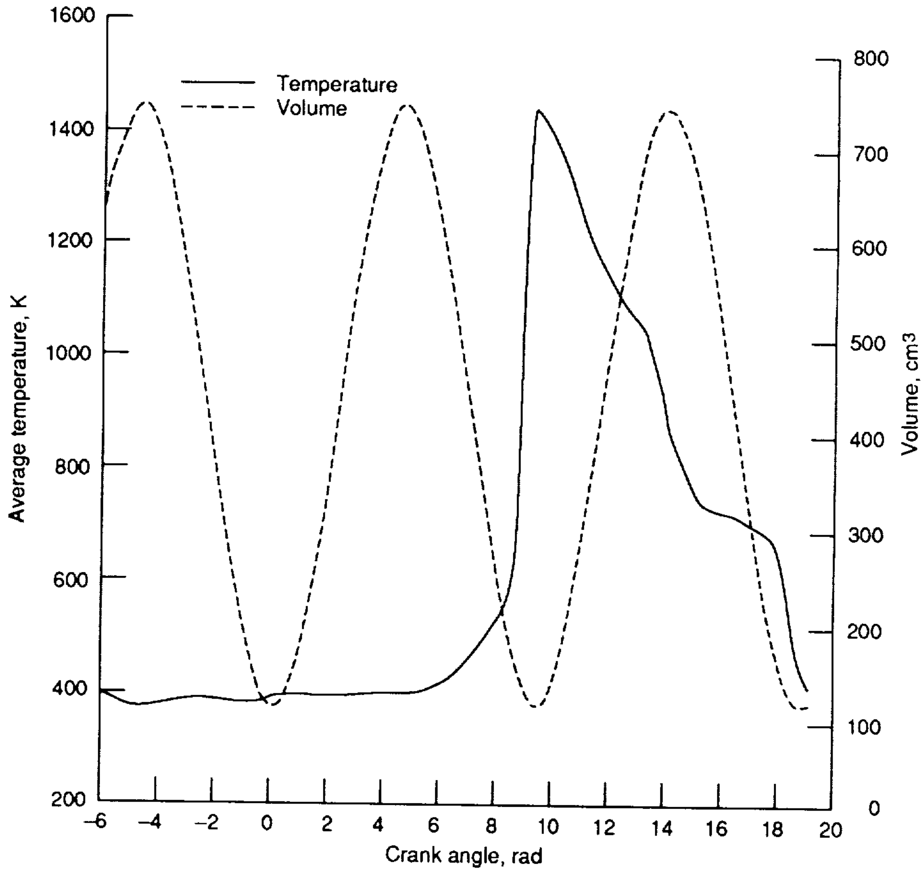

(b) Temperature and volume versus crank angle.

Figure 5.—Pressure, temperature, and volume histories for $\Phi = 0.45$.

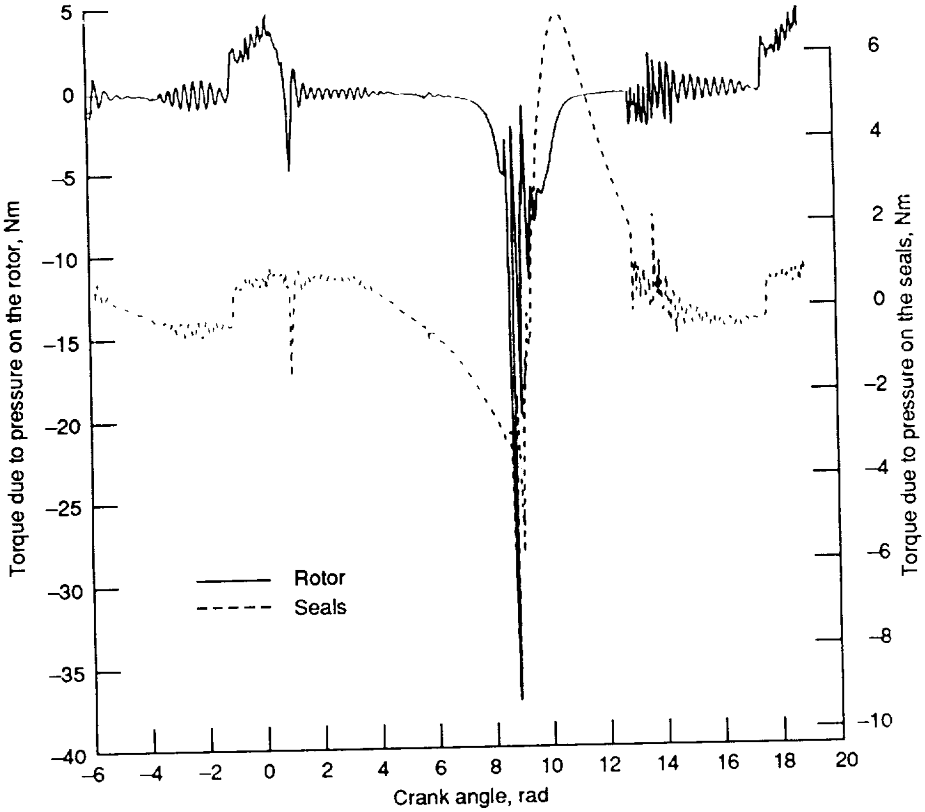

(a) Torque versus crank angle.

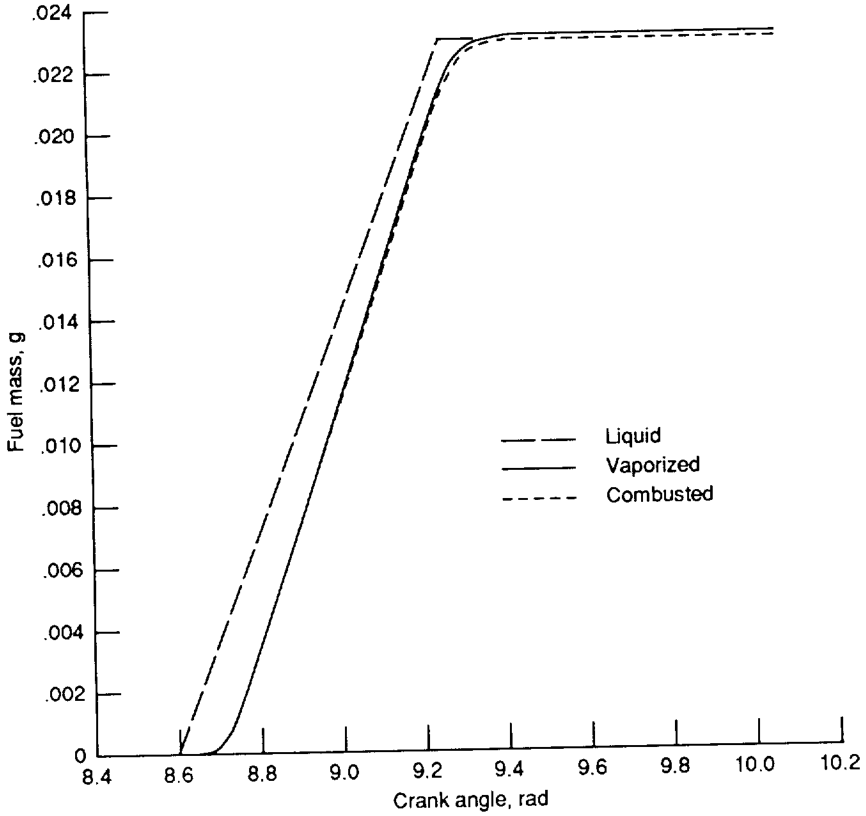

(b) Variation of amounts of fuel evaporated and reacted.

Figure 6.—Torque and fueling histories with $\Phi = 0.45$.

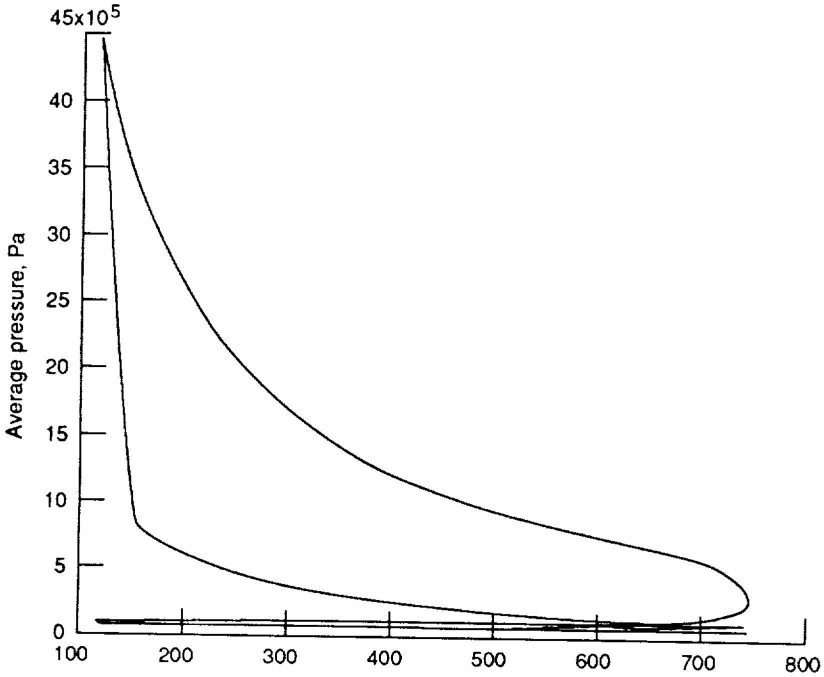

(a) Pressure versus volume.

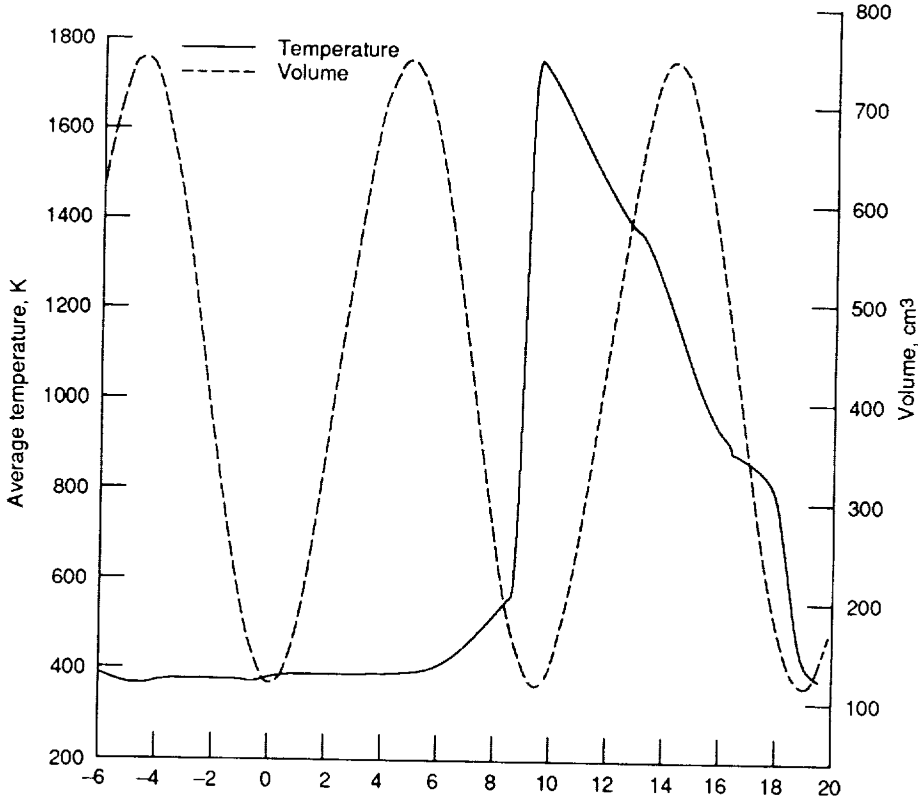

(b) Temperature and volume versus crank angle.

Figure 7.—Pressure, temperature, and volume histories for $\Phi = 0.75$.

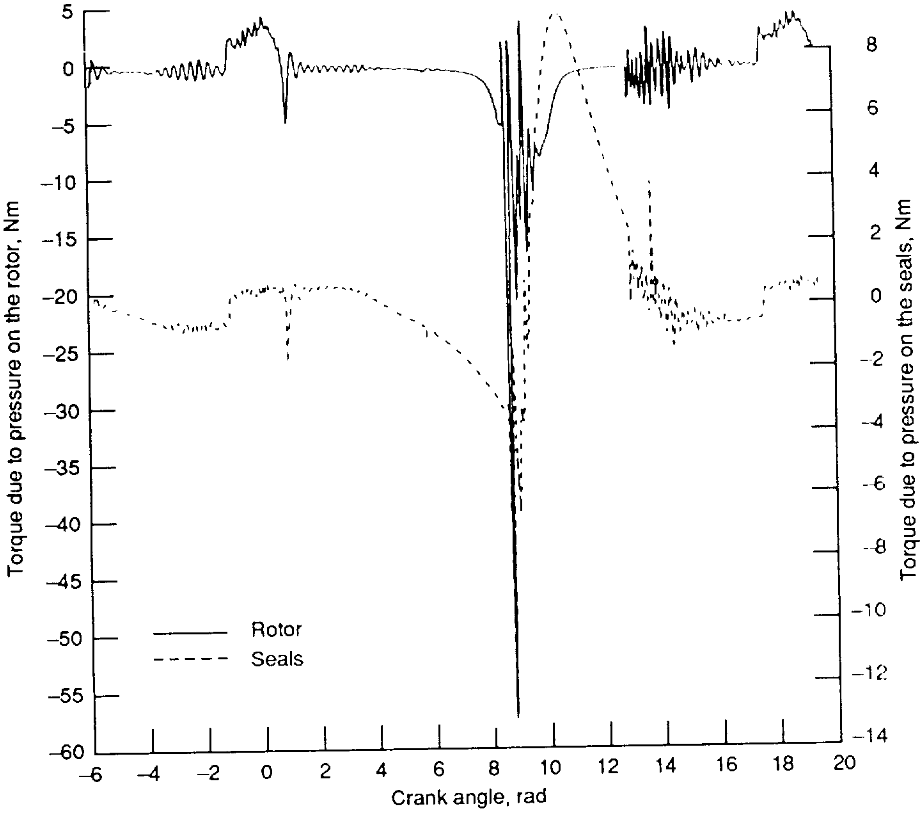

(a) Torque versus crank angle.

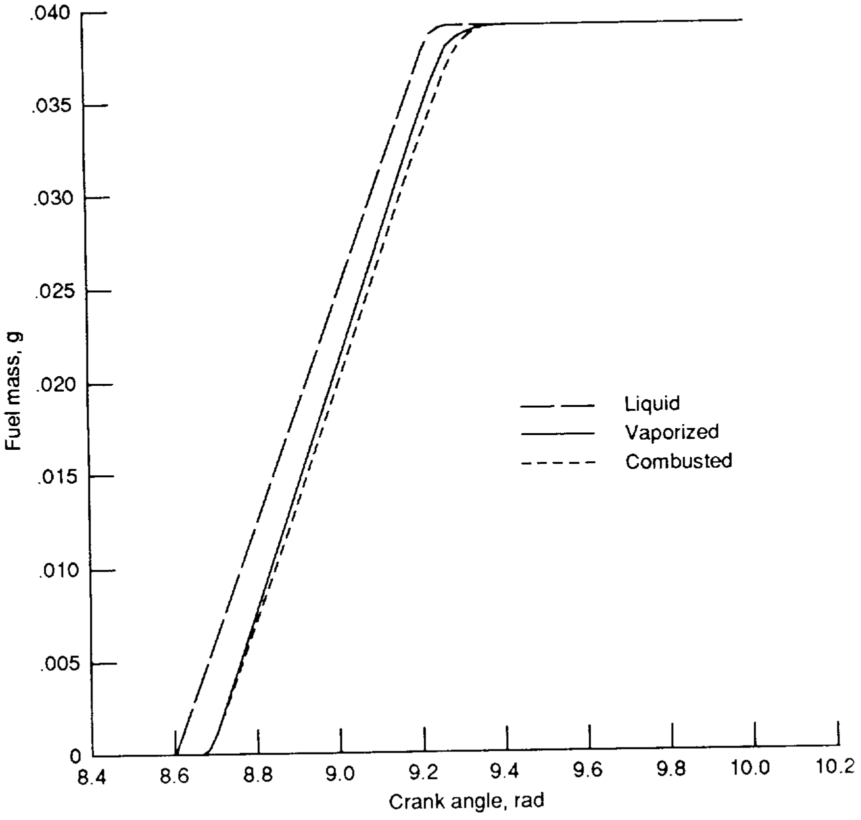

(b) Variation of amounts of fuel evaporated and reacted.

Figure 8.—Torque and fueling histories with $\Phi = 0.75$.

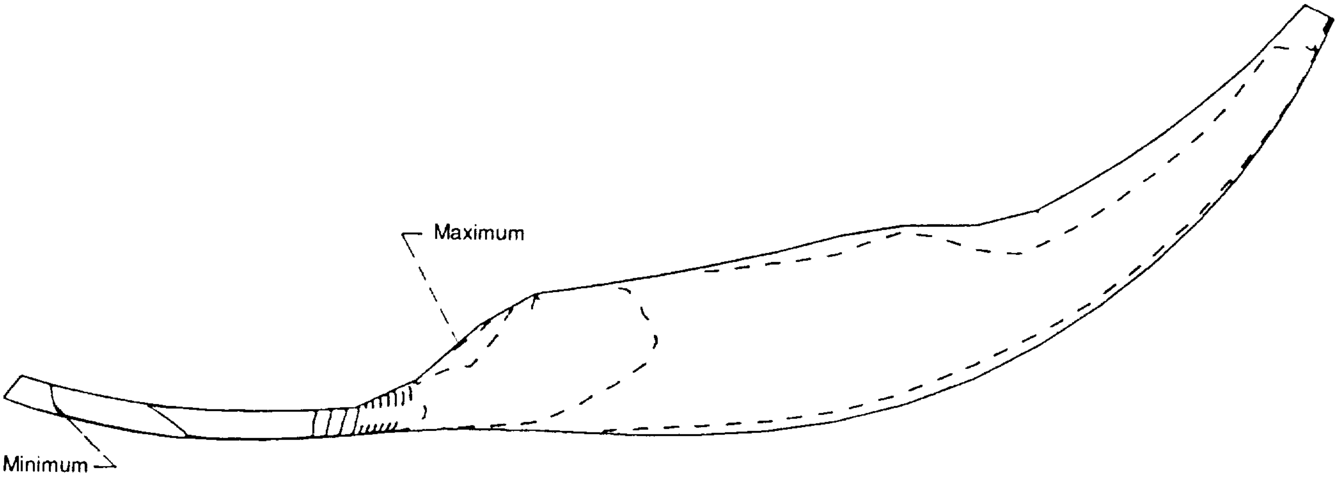

(a) Pressure contours (P_{max} = 0.80x10^6, P_{min} = 0.76x10^6, and ΔP = 0.26x10^4).

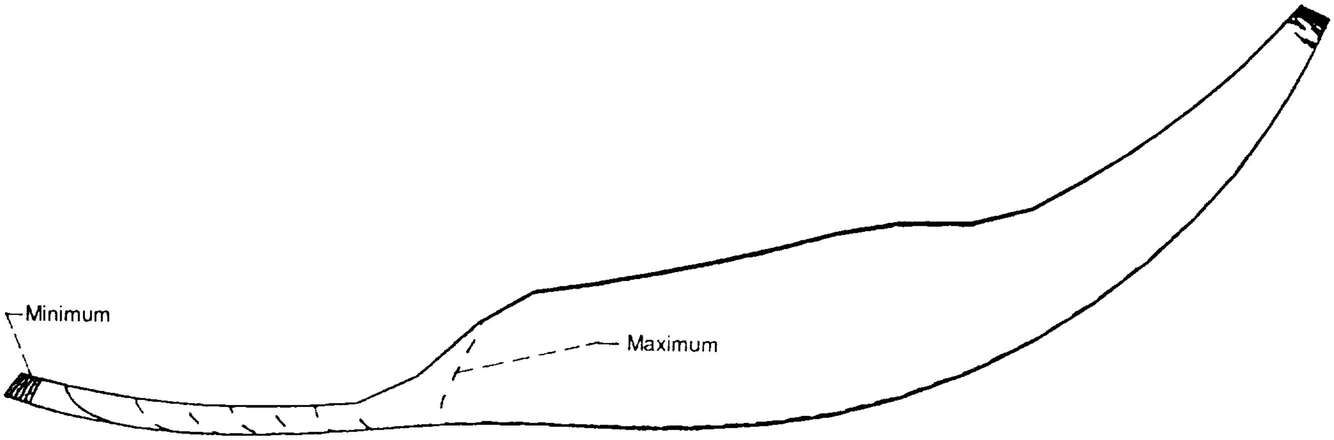

(b) Temperature contours (T_{max} = 606.1, T_{min} = 400.0, and ΔT = 15).

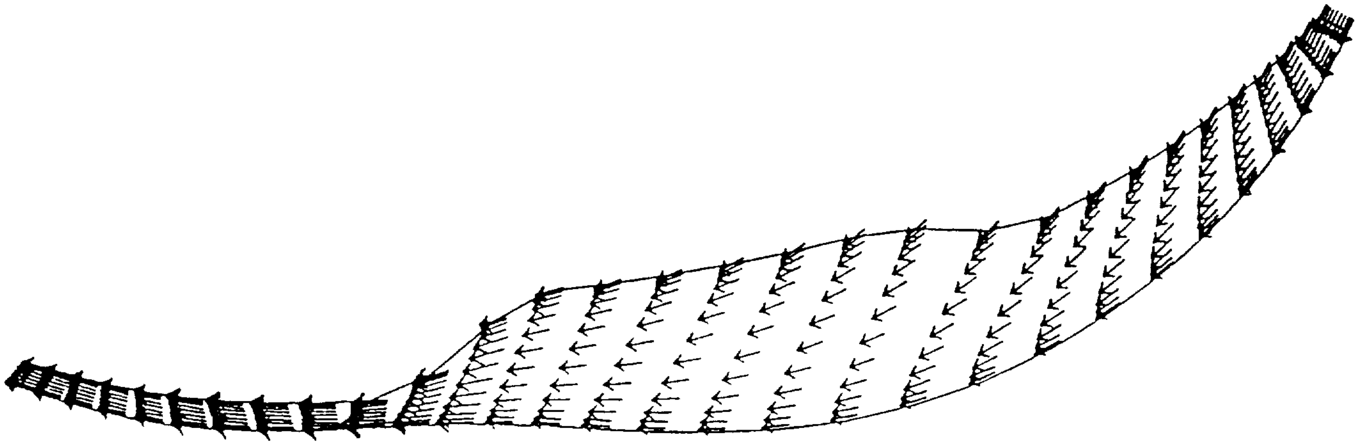

(c) Velocity vector plot (V_{max} = 35.34 m/s).

Figure 9.—Gas pressure, temperature, and velocity at θ = 8.6 rad and K = 9 for the case with Φ = 0.75.

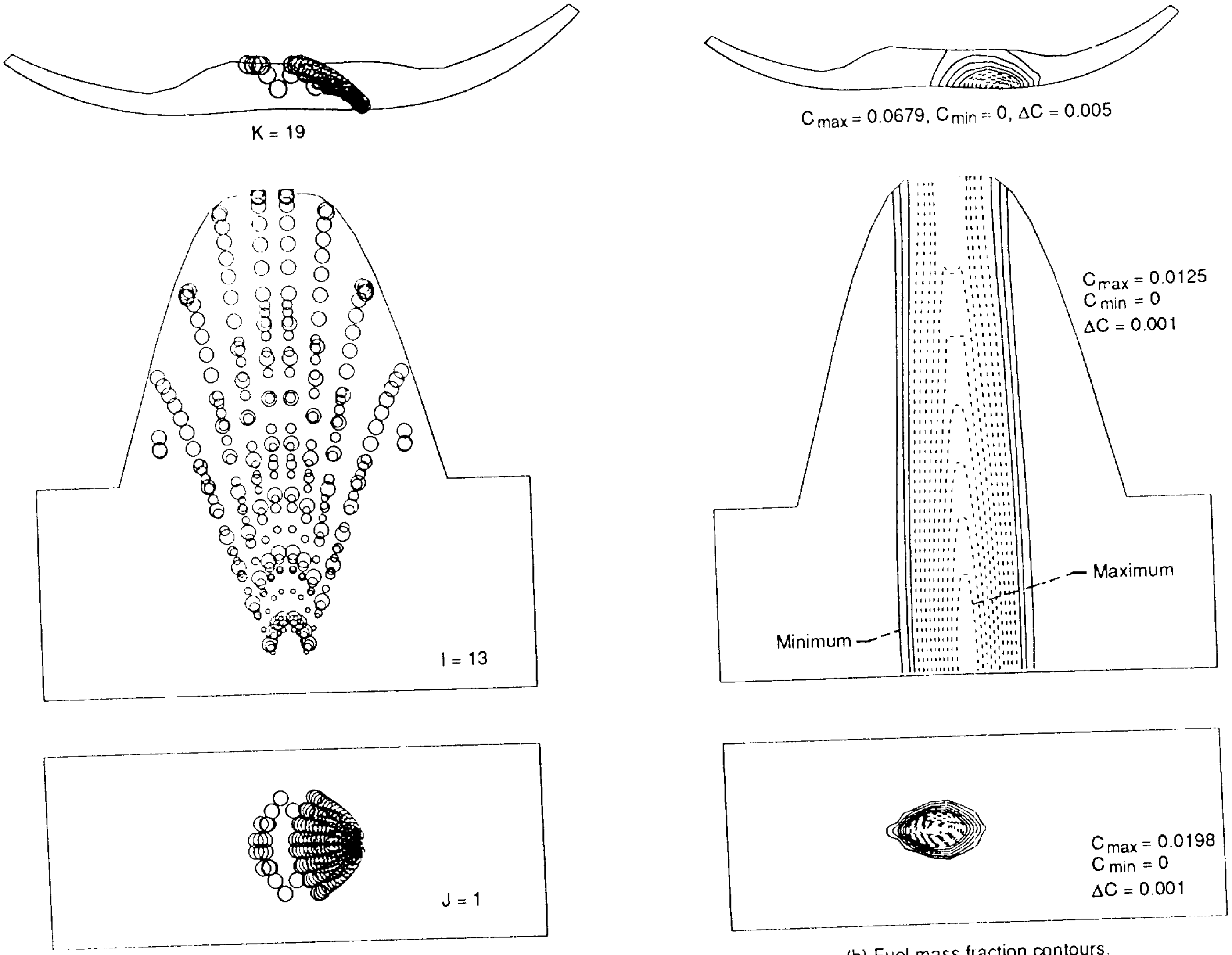

(a) Droplet trajectories.

(b) Fuel mass fraction contours.

Figure 10.—Droplet trajectories and fuel mass fraction contours at $\theta = 9.3$ rad for $\Phi = 0.75$.

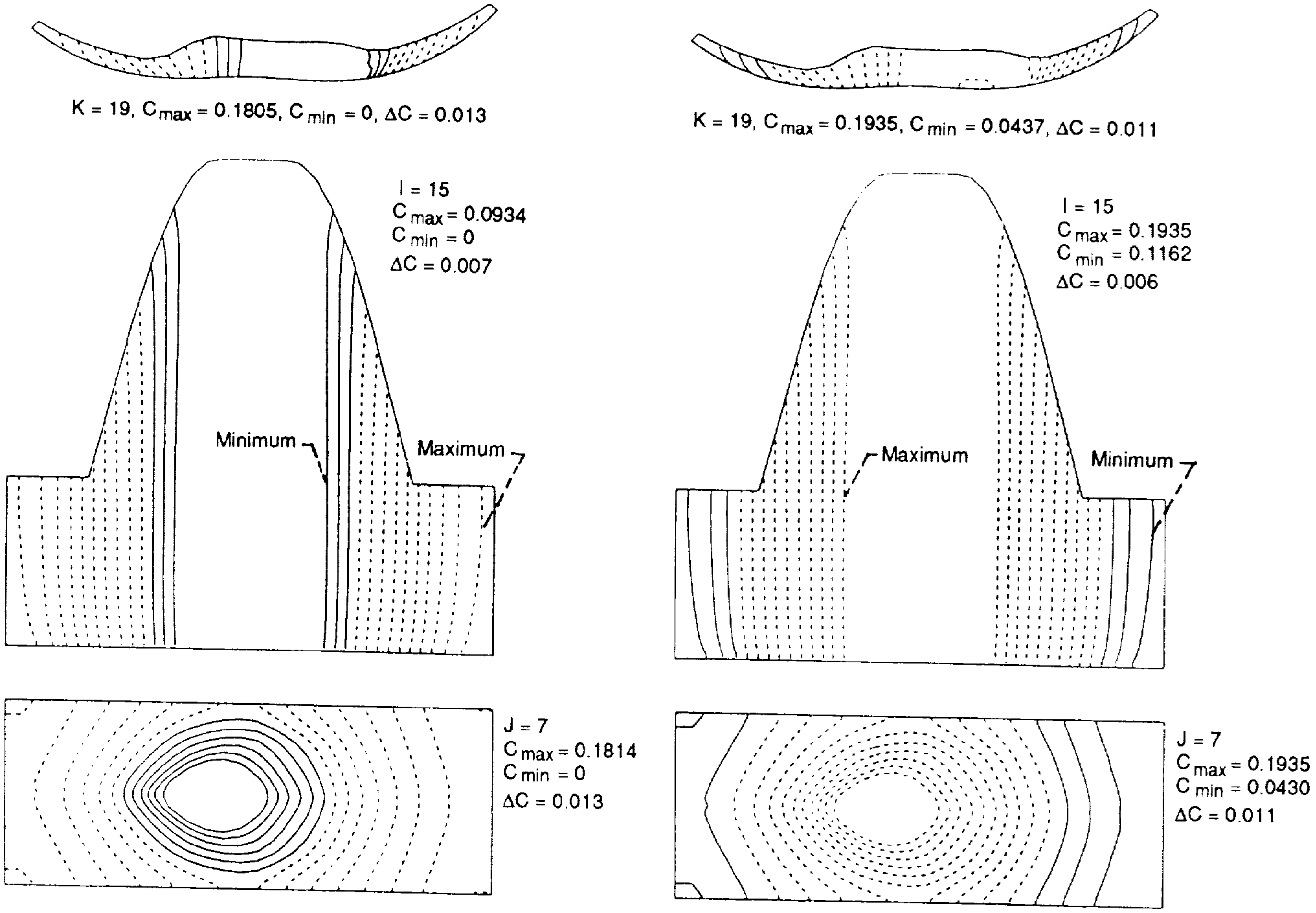

(a) Oxygen mass fraction contours.

(b) Carbon dioxide mass fraction contours.

Figure 11.—Oxygen and carbon dioxide mass fraction contours at θ = 9.3 rad for Φ = 0.75.

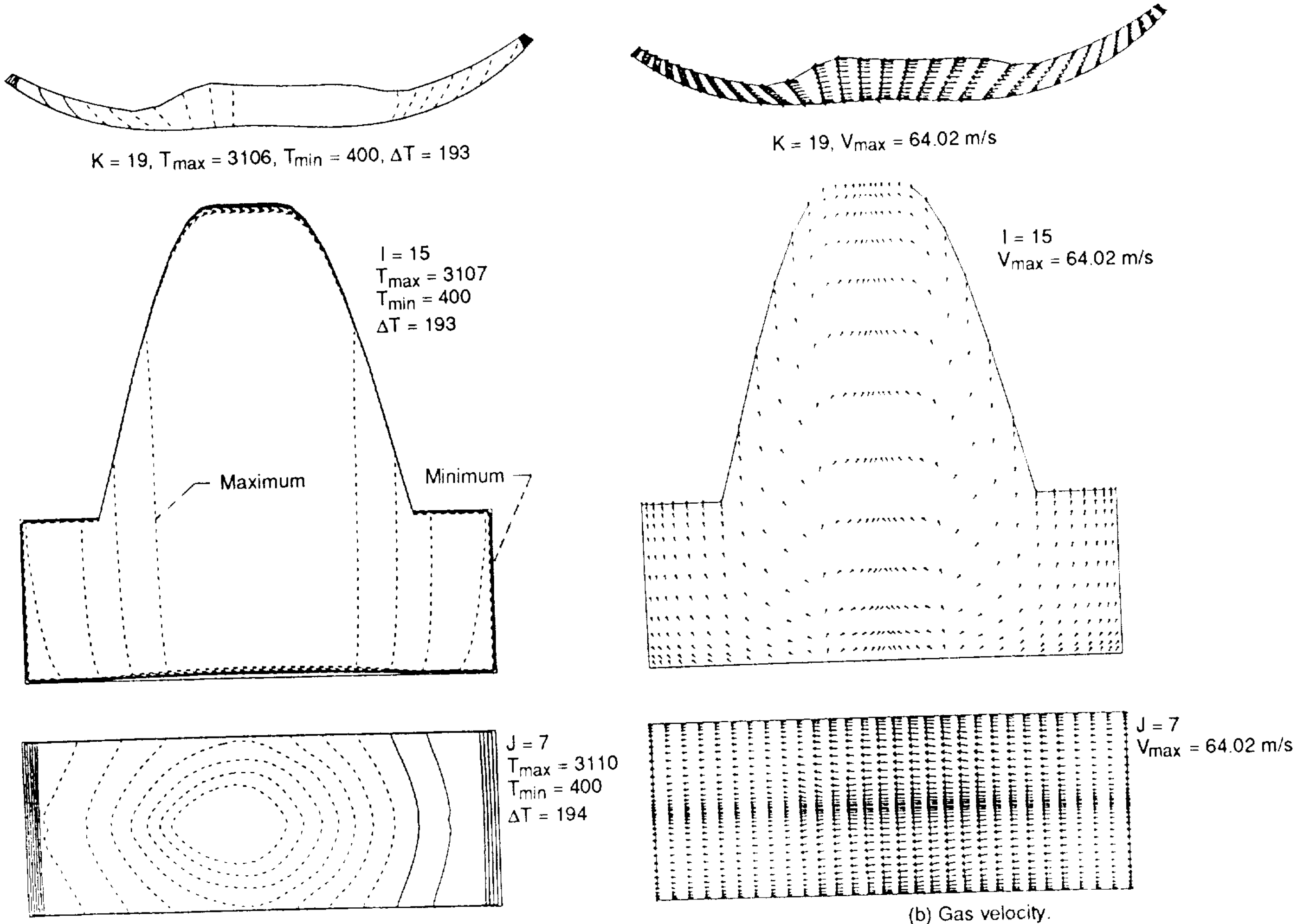

(a) Isotherms.

(b) Gas velocity.

Figure 12.—Isotherms and gas velocity at θ = 9.3 rad for Φ = 0.75.

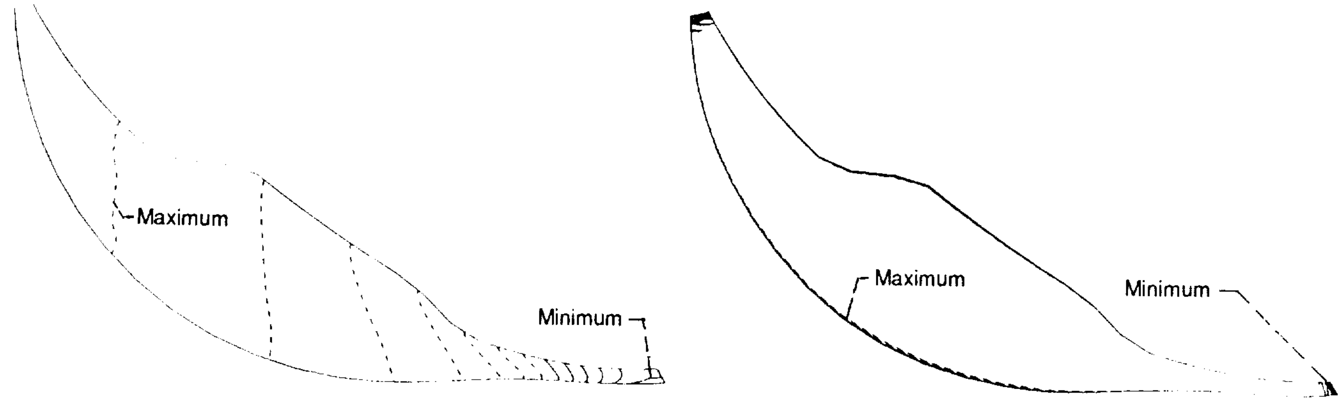

(a) Oxygen concentration contours (C_{max} = 0.0923, C_{min} = 0.0895, and ΔC = 0).

(c) Temperature contours (T_{max} = 2017, T_{min} = 400, and ΔT = 116).

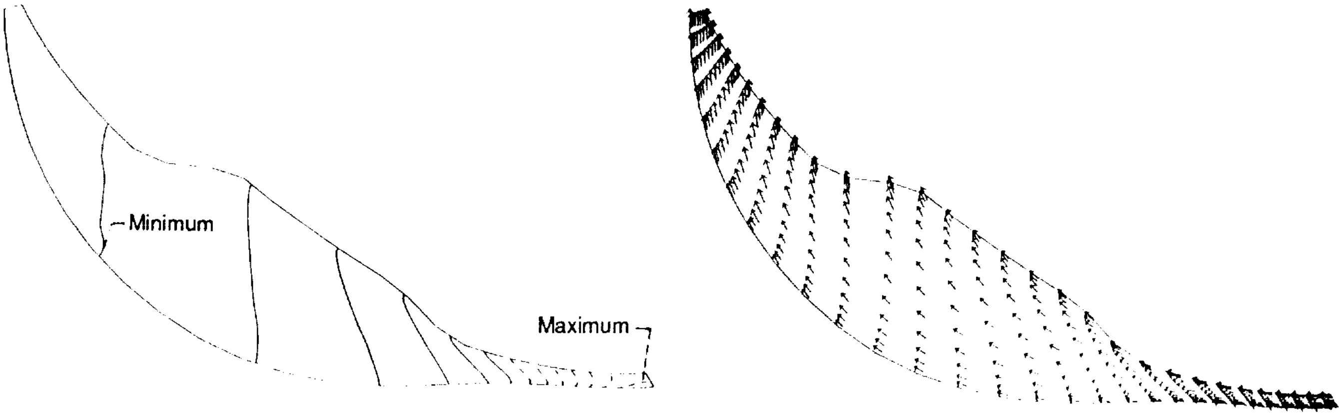

(b) Carbon dioxide concentration (C_{max} = 0.1194, C_{min} = 0.1171, and ΔC = 0).

(d) Velocity vector plot (V_{max} = 21.85 m/s).

Figure 13.—Oxygen, carbon dioxide, and temperature contours and gas velocity at θ = 11 rad and K = 19 for Φ = 0.75.

National Aeronautics and Space Administration

Report Documentation Page

1. Report No.
NASA TM-103104

2. Government Accession No.

3. Recipient's Catalog No.

4. Title and Subtitle
Computational Experience With a Three-Dimensional Rotary Engine Combustion Model

5. Report Date

6. Performing Organization Code

7. Author(s)
M.S. Raju and E.A. Willis

8. Performing Organization Report No.
E-5249

10. Work Unit No.
505-62-11

9. Performing Organization Name and Address
National Aeronautics and Space Administration
Lewis Research Center
Cleveland, Ohio 44135-3191

11. Contract or Grant No.

13. Type of Report and Period Covered
Technical Memorandum

12. Sponsoring Agency Name and Address
National Aeronautics and Space Administration
Washington, D.C. 20546-0001

14. Sponsoring Agency Code

15. Supplementary Notes
Prepared for the Joint Symposium on General Aviation Systems cosponsored by the AIAA and FAA, Ocean City, New Jersey, April 11-12, 1990. M.S. Raju, Sverdrup Technology, Inc., Lewis Research Center Group, 2001 Aerospace Parkway, Brook Park, Ohio 44142. (Work funded by NASA Contract NAS3-25266.) E.A. Willis, NASA Lewis Research Center.

16. Abstract

A new computer code has been developed to analyze the chemically reactive flow and spray combustion processes occurring inside a stratified-charge rotary engine. Mathematical and numerical details of the new code were recently described by the present authors. This paper presents the results of limited, initial computational trials as a first step in a long-term assessment/validation process. The engine configuration studied was chosen to approximate existing rotary engine flow-visualization and hot-firing test rigs. Typical results include (1) pressure and temperature histories, (2) torque generated by the nonuniform pressure distribution within the chamber, (3) energy release rates, and (4) various flow-related phenomena. These are discussed and compared with other predictions reported in the literature. The adequacy or need for improvement in the spray/combustion models and the need for incorporating an appropriate turbulence model are also discussed.

17. Key Words (Suggested by Author(s))
Rotary engine
Combustion
Fuel injection
Computational fluid mechanics

18. Distribution Statement
Unclassified – Unlimited
Subject Category 34

19. Security Classif. (of this report)
Unclassified

20. Security Classif. (of this page)
Unclassified

21. No. of pages
24

22. Price*
A03

NASA FORM 1626 OCT 86

*For sale by the National Technical Information Service, Springfield, Virginia 22161